GEOPHYSICS

Discriminating between natural versus induced seismicity from long-term deformation history of intraplate faults

Maria Beatrice Magnani,[1]* Michael L. Blanpied,[2] Heather R. DeShon,[1] Matthew J. Hornbach[1]

To assess whether recent seismicity is induced by human activity or is of natural origin, we analyze fault displacements on high-resolution seismic reflection profiles for two regions in the central United States (CUS): the Fort Worth Basin (FWB) of Texas and the northern Mississippi embayment (NME). Since 2009, earthquake activity in the CUS has increased markedly, and numerous publications suggest that this increase is primarily due to induced earthquakes caused by deep-well injection of wastewater, both flowback water from hydrofracturing operations and produced water accompanying hydrocarbon production. Alternatively, some argue that these earthquakes are natural and that the seismicity increase is a normal variation that occurs over millions of years. Our analysis shows that within the NME, faults deform both Quaternary alluvium and underlying sediments dating from Paleozoic through Tertiary, with displacement increasing with geologic unit age, documenting a long history of natural activity. In the FWB, a region of ongoing wastewater injection, basement faults show deformation of the Proterozoic and Paleozoic units, but little or no deformation of younger strata. Specifically, vertical displacements in the post-Pennsylvanian formations, if any, are below the resolution (~15 m) of the seismic data, far less than expected had these faults accumulated deformation over millions of years. Our results support the assertion that recent FWB earthquakes are of induced origin; this conclusion is entirely independent of analyses correlating seismicity and wastewater injection practices. To our knowledge, this is the first study to discriminate natural and induced seismicity using classical structural geology analysis techniques.

INTRODUCTION

A fundamental question about continental intraplate seismicity is why it occurs where it does. Most earthquakes are associated with preexisting structures post facto, but because continents contain many such structures, it is difficult to predict which ones will become active. Hence, it is important to know whether, over time, seismicity continues on structures that are most active at present, or whether modern seismicity is a rejuvenation of long-dormant faults. This issue is scientifically important, has a crucial impact on seismic hazard assessment, and has been given new urgency because of the recent increase in the rate of seismicity associated with subsurface wastewater injection in the North America intraplate region (*1*–*3*).

The brittle crust in continental interiors is in frictional failure equilibrium (that is, shear stresses are near the strength limit of the crust) and faults are critically stressed (*4*, *5*). Because strain rates in these regions are generally quite low (10^{-17} s^{-1} or less) (*6*, *7*), long-term fault slip rates are quite slow (<<1 mm/year) (*8*), with the result that recurrence intervals of continental intraplate earthquakes can be on the order of 10,000 to 100,000 years (*9*, *10*) and stress can reactivate ancient faults that are not associated with historic seismicity. Also, because strain builds slowly, stress perturbations imparted by processes in addition to plate motion (for example, traction from mantle flow, regional loads such as glacial isostatic adjustment and sediment denudation, or high-pressure fluid injection) might control deformation, with the result that intraplate seismicity often migrates between faults and is episodic and clustered (*11*, *12*).

The central United States (CUS) has a record of historical seismicity that dates back to late 1700s when felt reports were first documented in the midcontinent. Pre-2008 seismicity in the CUS is scattered and dominated by two source regions: the New Madrid seismic zone (NMSZ) in the Mississippi River valley and the east Tennessee seismic zone along the southern Appalachian Mountains. Since about 2009, however, the CUS has witnessed both a dramatic increase in the rate of seismicity and a marked change in its spatial distribution (Fig. 1). Earthquakes now occur in regions that had little or no seismicity before 2009, whereas previously active areas have maintained nearly constant earthquake rates (*1*, *13*). This change is unprecedented in both areal extent and rate, and has increased seismic hazard in the region (*14*). A major fraction of this anomalous seismicity has occurred in areas of hydrocarbon production and related wastewater injection, suggesting that the earthquakes may be caused by industry practices (for example, through reduction of effective stresses on faults or by stress perturbation in the crust) [(*1*, *14*, *15*) and references therein].

The discrimination between seismic activity that is anthropogenically induced and that which arises from natural tectonic deformation is therefore of critical importance, because seismic hazard resulting from human activity can potentially be mitigated. In addition, the discrimination provides a window into the state of stress of intraplate faults and into seismicity in stable continental regions and the processes that drive it.

There are two possible causes for the recent seismicity in intraplate regions like the CUS. One possibility is that it represents natural tectonic activity along intraplate faults deforming at low strain rates via infrequent (thousands of years) bursts of activity that are not fully captured by the relatively short (tens of years) span of instrumental monitoring or historical record. The second possibility is that human activities are reactivating and inducing slip on long-dormant faults, which would otherwise have remained inactive.

Discriminating between these two cases is particularly challenging because often the causative faults are unknown or poorly known and have no surface expression, especially if seismicity occurs on or reactivates

[1]Roy Huffington Department of Earth Sciences, Southern Methodist University, Dallas, TX 75205, USA. [2]U.S. Geological Survey Earthquake Hazard Program, Reston, VA 20192, USA.
*Corresponding author. Email: mmagnani@smu.edu

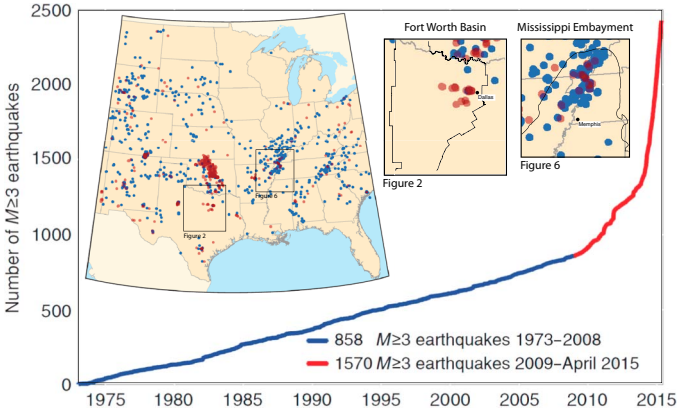

Fig. 1. Post-2008 seismicity rate change in the CUS. The post-2008 seismicity has occurred both in areas that were seismically active before 2008 (for example, the Mississippi embayment) and in regions with no pre-2008 historical or instrumental seismicity (for example, FWB). The two study areas are outlined and represented in Figs. 2 and 6. Modified with permissions from Rubinstein and Mahani (*13*).

ancient faults in the Proterozoic basement (*2*, *16*, *17*). Most investigations concerning the causal factors of the recent CUS seismicity are based on observations that are limited to the few years of wastewater injection (for example, in the case of pore pressure diffusion modeling) (*18*–*20*) or to the few tens of years of historical and instrumental record (in the case of seismicity) (*1*–*3*, *16*, *17*, *21*, *22*). Although these investigations contribute essential elements to the study of the relationship between anthropogenic activity and seismicity, and to an understanding of the processes involved, the long-term information on the causative faults is missing.

Here, we demonstrate how seismic reflection data, by elucidating the existence, distribution, orientation, and dimension of faults, provide irreplaceable information to establish fault susceptibility for reactivation either by injection or by tectonic processes, and can be used to evaluate the potential maximum size of an earthquake. Using classical geology analysis techniques, we show how, by evaluating displacement history over the lifetime of the fault, seismic reflection data contribute information that complements analyses of contemporary seismicity and, independently of wastewater injection modeling, can help to discriminate whether earthquake sequences have an induced or a natural origin.

To illustrate this, we evaluate fault deformation history from two regions in the CUS: (i) the Fort Worth Basin (FWB) of north Texas, where historical (~1850) seismic activity began only in 2008 (*21*, *23*) and is spatially associated with a region of intense exploitation of unconventional oil and gas sources and of wastewater disposal (*24*), and (ii) the northern Mississippi embayment (NME), where paleoseismic observations show seismicity during the late Pleistocene (*25*) and the Holocene (*26*) throughout the region. Both the FWB and the NME have a rich tectonic history that dates back to the Paleozoic, are currently seismically active, and are covered by post-Paleozoic sediments and sedimentary rocks that conceal the causative faults. In both basins, we examine long-term fault displacement as imaged by seismic reflection profiles across faults currently active and quiescent. In the NME, we show that, along faults that are currently seismically active, motion has been occurring over many millions of years. In the FWB, along faults that are currently seismically active, there is no evidence of previous motion over the past millions of years, suggesting that the current earthquakes are induced.

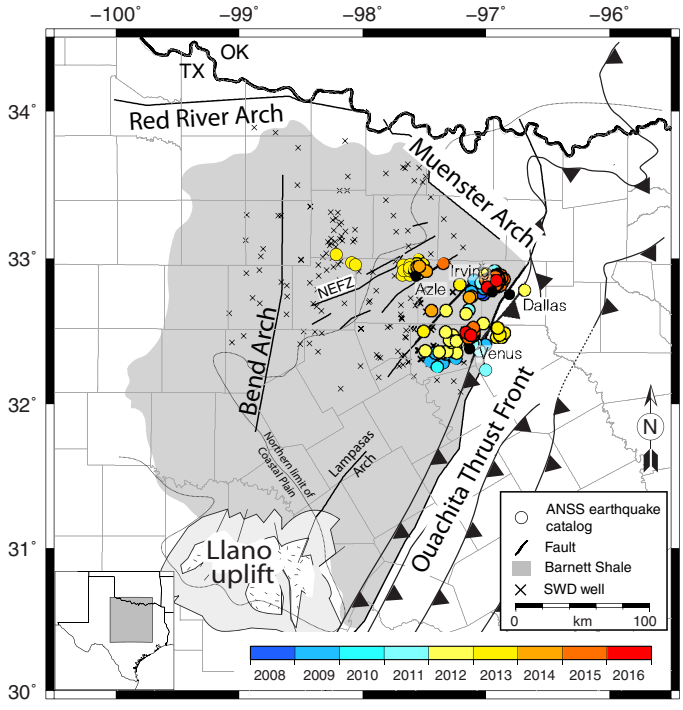

Fig. 2. Earthquakes in the FWB, north Texas. The map shows the main tectonic features of the basin, instrumental seismicity ($1.8 > M_w > 4.0$), and the geographical extent of the Barnett Shale, the main oil and gas production unit. Produced brine and wastewater associated with stimulation of unconventional reservoirs are reinjected through deep wells (that is, saltwater disposal well; crosses in figure) in the Ellenburger Group, below the Barnett Shale. NEFZ, Newark east fault zone; SWD, saltwater disposal. Llano uplift, stipple pattern–Precambrian metasedimentary rocks; light gray, Ordovician carbonates. Seismicity shows clusters around Azle (Parker County), Irving-Dallas (Dallas County), and Venus (Johnson County). Faults from Ewing *et al.* (*36*).

RESULTS

The Fort Worth Basin

Recent seismic activity

Between 2008 and 2016, the rate of earthquakes with magnitude greater than 3 in Texas has increased from 2 to 12 per year (*22*, *23*, *27*). Rate changes have been highest in northeast and west Texas, regions of intense exploitation for unconventional oil and gas sources and large volume wastewater disposal (*15*, *23*, *27*, *28*). In one of the most active regions, the FWB of north Texas, the U.S. Geological Survey (USGS) National Earthquake Information Center (NEIC) catalog reports more than 200 earthquakes, with at least 32 events of magnitude greater than 3 and one magnitude 4 (Fig. 2). Dedicated local seismic networks deployed in the basin from 2013 to present have recorded more than 1300 earthquakes of magnitude between −1.0 and 4.0 [(*29*), hereafter the Southern Methodist University (SMU) catalog]. Since 2008, there have been five well-studied earthquake sequences: 2008–2009 Dallas/Fort Worth International Airport (*21*), 2009 Cleburne (*27*), 2013–2015 Azle-Reno (*19*), 2014–2016 Irving-Dallas (*30*, *31*), and 2008–2016 Venus (*22*, *32*). Sequences occur within or nearby a region of increased wastewater injection volumes into the Early Ordovician Ellenburger Group (*28*). Hypocentral depths range from 2 to 8 km, that is, within the Precambrian granitic basement, in contact with the carbonates of the Ellenburger, and only with limited cases of seismicity in the Ordovician units (*19*). Causative faults in the crystalline basement, as illuminated by seismicity, strike north-northwest

(NNW)–south-southwest (SSW) and northeast (NE)–southwest (SW), dip 40° to 70° to the southeast (SE) and NW, and extend for 2 to 6 km in length and 4 to 8 km in depth, resulting in fault areas of 10 to 15 km^2 (*19*, *22*, *32*, *33*). Focal mechanisms show consistently normal faulting throughout the eastern [Advanced National Seismic System (ANSS) Comprehensive Catalog] and north-central parts of the FWB (*19*).

Tectonic setting

The FWB is a north-south elongated foreland basin that developed during the later part of the Paleozoic along the southwest border of the advancing front of the Ouachita fold-and-thrust belt (Fig. 2) (*34*). The basin is bordered to the north and east by fault-controlled basement uplifts (Red River and Muenster arches and the Ouachita fold-and-thrust belt, respectively) and to the south by a crystalline basement–cored dome (Llano uplift). To the west, the basin shallows over a broad, north-plunging, positive structure, the Bend Arch, which formed by flexure of the basin to the east under the Ouachita fold-and-thrust belt (*35*).

The tectonic events that defined the boundaries of the FWB appear to have also controlled the main structures of the basin. Minor and major high-angle normal faults are interpreted from drill data and seismic reflection profiles throughout the basin, and their orientations vary and align with the major tectonic elements, suggesting a genetic relationship. In the central and eastern parts of the FWB, where most of the recent seismicity has occurred, faults trend NNE-SSW, parallel to the Ouachita fold-and-thrust front (*34*, *36*), suggesting a relationship with this orogenic structure. NE-SW trending faults continue to the southern half of the basin, following the Lampasas Arch, consistent with the Ouachita fold-and-thrust belt trend, and are mapped on the Llano uplift. The eastward thickening of the foreland sequences is assisted by normal faults parallel to the leading edge of the Ouachita belt. These faults accommodated the flexure of the platform and the rapid subsidence that began in the Late Mississippian and continued throughout the orogenic phase as the margin was progressively loaded by the encroaching Ouachita fold-and-thrust belt.

Preserved sedimentary rocks in the central-eastern FWB (Fig. 3) consist of ~1200 to 1500 m of Ordovician passive margin carbonates (that is, Ellenburger Group, Simpson Group, and Viola Limestone) deposited between 490 and 360 Ma (million years ago) above the Precambrian crystalline basement and the Upper Cambrian Riley Formation (which includes the highly friable Hickory Sandstone Member at its base) and Wilberns Formation, Middle-Upper Mississippian and Lower-Middle Pennsylvanian shales and carbonates (that is, Chappel Limestone, Barnett Shale, and Marble Falls Limestone of the Bend Group) ranging in ages between 360 and 310 Ma, and Pennsylvanian siliciclastic foredeep units (that is, Bend and Strawn Groups) deposited during the time interval of 310 to 299 Ma. Permian units are prevalent west of the Bend Arch but not present in the eastern FWB. Along the eastern portion of the basin, southeastward thickening Cretaceous coastal plain sediments rest unconformably over eastward dipping eroded Paleozoic sequences, marking the incursion of the Early Cretaceous seas (*35*).

The Mississippian Barnett Shale is the main source rock for gas and oil produced in the FWB, and it is also the main production horizon within the Barnett Paleozoic total petroleum system (*24*). Production from this horizon increased from 2000 to 2016 due to the success of unconventional stimulation of fields through hydraulic fracturing of tight shales (*37*). The flowback wastewater and the highly saline water produced from the fracturing process have been disposed in increasing volumes in the basin via reinjection in deep wells that penetrate the Ordovician carbonates (that is, Ellenburger) above the Late Cambrian Hickory Sandstone Member of the Riley Formation and the crystalline basement (*15*, *28*).

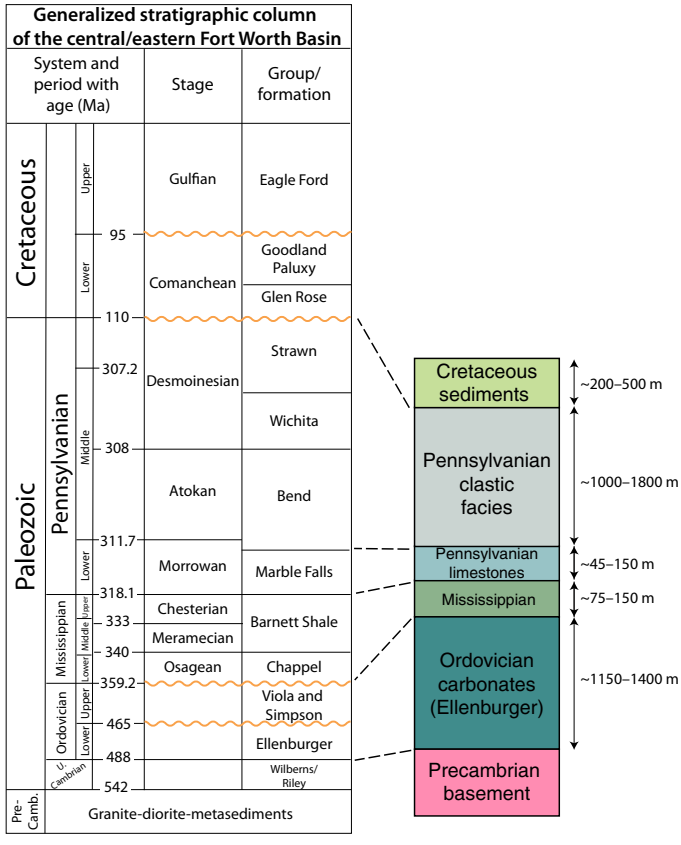

Fig. 3. Generalized subsurface stratigraphic section of the central and eastern FWB. Most of the saltwater disposal in the FWB takes place in the Early Ordovician Ellenburger Group, close to the Precambrian basement where the majority of seismicity occurs. Few wells penetrate below the Ellenburger, and details of the Cambrian stratigraphy are from the Llano uplift, central Texas. The schematic stratigraphic column to the right shows the main horizons identified in the seismic reflection profiles shown in Figs. 4 and 5. Modified with permissions from Pollastro *et al.* (*24*) and Ewing (*97*).

Fault displacement history

Because of decades of extensive hydrocarbon exploration and production, a wealth of data has been gathered in the FWB that constrains the tectonic structure, evolution, and subsurface architecture of the economically relevant units (for example, Barnett Paleozoic total petroleum system). Unfortunately, however, detailed knowledge of the faults that dissect the Paleozoic sedimentary fill and the crystalline basement relies predominantly on geological mapping from outcrops on the Llano uplift at the southern margin of the FWB and on proprietary two-dimensional (2D) and 3D seismic reflection data that are rarely published (*38*, *39*) or available for consultation. Early published work in the basin supports the existence of several faults identified by well-log correlations and structural mapping at the Early Ordovician Ellenburger Group stratigraphic level that cut basement and Lower Paleozoic rocks. Evidence shows that these faults and associated structures formed during the development of the Llano uplift and the FWB, with faulting extending

upward through the limestone of the Marble Falls (Lower Pennsylvanian, ~320 Ma) (*40*, *41*).

To our knowledge, there is no published seismic reflection data set across the structures that host the current seismicity in the FWB that images in detail the fault geometry and long-term deformation history. Below, we describe two examples of proprietary commercial 2D and 3D seismic reflection data sets that image the currently active faults near Venus and Irving-Dallas, along the eastern margin of the FWB. Here, seismicity initiated and evolved on structures subparallel to the Ouachita orogenic front (Fig. 2).

Analysis of high-resolution seismic reflection data

Venus, Texas, area

Seismicity in the Venus area (Johnson County) occurs in a county with long-term, high-volume wastewater disposal (*28*). The area experienced a M_w (moment magnitude) 4.0 on 7 May 2015, the largest magnitude instrumental and historical reported earthquake in the FWB as of 2017. The moment tensor for this event indicates normal faulting, and hypocenters, limited to the basement within a depth of 4 to 8 km, identify a west-dipping nodal plane striking ~230°N as the causative fault (*32*). Waveform template matching analysis indicates that seismic activity on this fault extends back to 2008 and that maximum magnitude increases with time, suggesting an ongoing seismic sequence and evolving slip rather than a mainshock-aftershock sequence (*32*).

Structural control and geometry (for example, length, dip, and strike) of the faults hosting the seismicity in the Venus area are constrained by three proprietary 2D seismic lines totaling 32 km (Fig. 4). The data were shot in 1964 and 1974 using a dynamite source and recorded to a maximum length of 7 s. Originally processed to time stack domain, in 2015 the data were reprocessed to prestack time migration. We subsequently depth-converted using a 1D velocity function calibrated on the stratigraphy derived from nearby well logs. The tops of the stratigraphic units were projected from wells onto the seismic profiles and correlated with main reflectors. The seismic data image the top of the crystalline basement, the Early Ordovician Ellenburger Group, the Mississippian-Lower Pennsylvanian shales and carbonates, and the Pennsylvanian clastic foreland units, which are all identified as the sequences downlapping onto the regional contact between the Bend Group (Atokan age, circa 310 Ma) sequences above and the Marble Falls Limestone below (Fig. 4). The base of the Lower Cretaceous coastal plain sediments is intermittently traceable at the top of all seismic profiles. Deformation of the Ordovician through Pennsylvanian sedimentary sequences is subtle, and two prominent oppositely dipping faults can be identified as offsetting the top of the east-dipping basement and penetrating the Ellenburger through the Mississippian shales. No offset or deformation of the reflector that marks the base of the Bend Group (~310 Ma age) and the overlying stratigraphy is resolved.

On the basis of the integrated interpretation of the three profiles, two faults [western Venus fault (WVF) and eastern Venus fault (EVF)] are interpreted to trend NE-SW (Fig. 4A). The WVF is interpreted as a west-dipping normal fault, at least 6.5 km long. Based on the constraints from the reflection data, the fault strikes ~210°N for about 4 km, consistent with the M_w 4.0 fault plane solution (~230°N), and then either rotates counterclockwise to the north or terminates northeast of line B. Most of the hypocentral locations of the Venus sequence cluster along the portion of the WVF plane that parallels the regional S_{Hmax} (Fig. 4) (*42*). We interpret the lack of seismicity to the north as a consequence of the fault becoming non-critically oriented within the modern stress field. Seismic reflection data show the EVF as a 25°N striking, steep east-dipping fault, with a down-to-the-east sense of motion. Unlike the WVF, there appears to be no seismicity ($M \geq 1.0$) associated with the EVF. The lack of resolved vertical displacement on both faults above the Atokan-age units (~310 Ma) indicates that these faults have not been active since the Pennsylvanian and until the start of the 2008 seismic swarm.

Irving-Dallas, Texas, area

Perhaps the most enigmatic sequence in the FWB, the Irving-Dallas earthquakes began in 2014 with a M_w 2.4 on 14 April and became highly productive with a set of five M_w 3.0+ events and a M_w 3.6 in January 2015. As with the Venus case, seismicity in the Irving-Dallas area is exclusively limited to the Precambrian basement (Fig. 5A), and the SMU catalog reports epicentral depths between 4.5 and 8 km, distributed on a 4-km-long plane striking ~39°N and dipping ~68° to the east (*30*).

Unlike the rest of the FWB seismic sequences, the Irving-Dallas sequence is not readily associated with nearby wells with long-term wastewater injection history. The nearest disposal well is located ~13 km to the northwest, and available records show fairly low injection volumes in the past decade (*28*). The only well operations near the Irving-Dallas sequence pertain to a set of inactive shale gas production wells (API 42-113-30147 and API 42-113-30189) at the southern end of the epicenter locations. Those two wells were drilled on the same pad and encountered the Ouachita orogen metasedimentary units under ~700 m of Cretaceous sediments before entering the Pennsylvanian foredeep facies. Documentation for the deepest well reports bottoming in the Ellenburger at a depth of 3070 m after penetrating the Marble Falls, the Barnett Shale at 2870 m, and the Viola-Simpson Group at a depth of 3014 m. Of the two wells, one failed in 2009 because of shallow casing failure during a hydrofracking stage and was shut in. The sole remaining producing well in the area ceased production in 2012 because of pipeline repairs. Despite its condition as a seismic outlier, Hornbach *et al.* (*28*) propose that the Dallas-Irving seismic sequence might also be induced by wastewater injection in light of its downslope position from Johnson County to the southwest (Fig. 2), which reports the largest injection volumes in the basin, directly along the basin structural axis and along the path of NE-SW trending basement faults that could act as fluid pathways and provide long-distance hydraulic connectivity.

We interpreted proprietary, unpublished, and processed 3D seismic reflection data acquired in 2008 with a Vibroseis source around the production wells. Data were interpreted in 3D, and faults were identified as reflector terminations/truncations and mapped in the data volume. The interpretation shows two southeast-dipping faults penetrating the base of the Barnett Shale, the Viola Limestone, and the Ellenburger Group with a down-to-the-east sense of motion (Fig. 5B). The faults displace the top of the basement reflector and are sealed at the top by the reflector, marking the upper part of the Marble Falls, as constrained by the well log at the center of the 3D volume footprint. Reflectors of the Pennsylvanian foredeep facies of the Bend Group, which show a characteristic prograding pattern with direction of transport from ESE to WNW, are continuous in the seismic data. Additional small-displacement west-dipping faults are visible at the top of the basement. These minor faults do not appear to penetrate the top of the Ellenburger. Horizontal time slices at the top of the basement show that basement structures (folds and faults) trend ~N40°E, parallel to the fault plane illuminated by the hypocentral locations (Fig. 5C) and consistent with the regional N20°E S_{Hmax} vector (*42*). Basement structures in the Dallas-Irving area trend parallel to

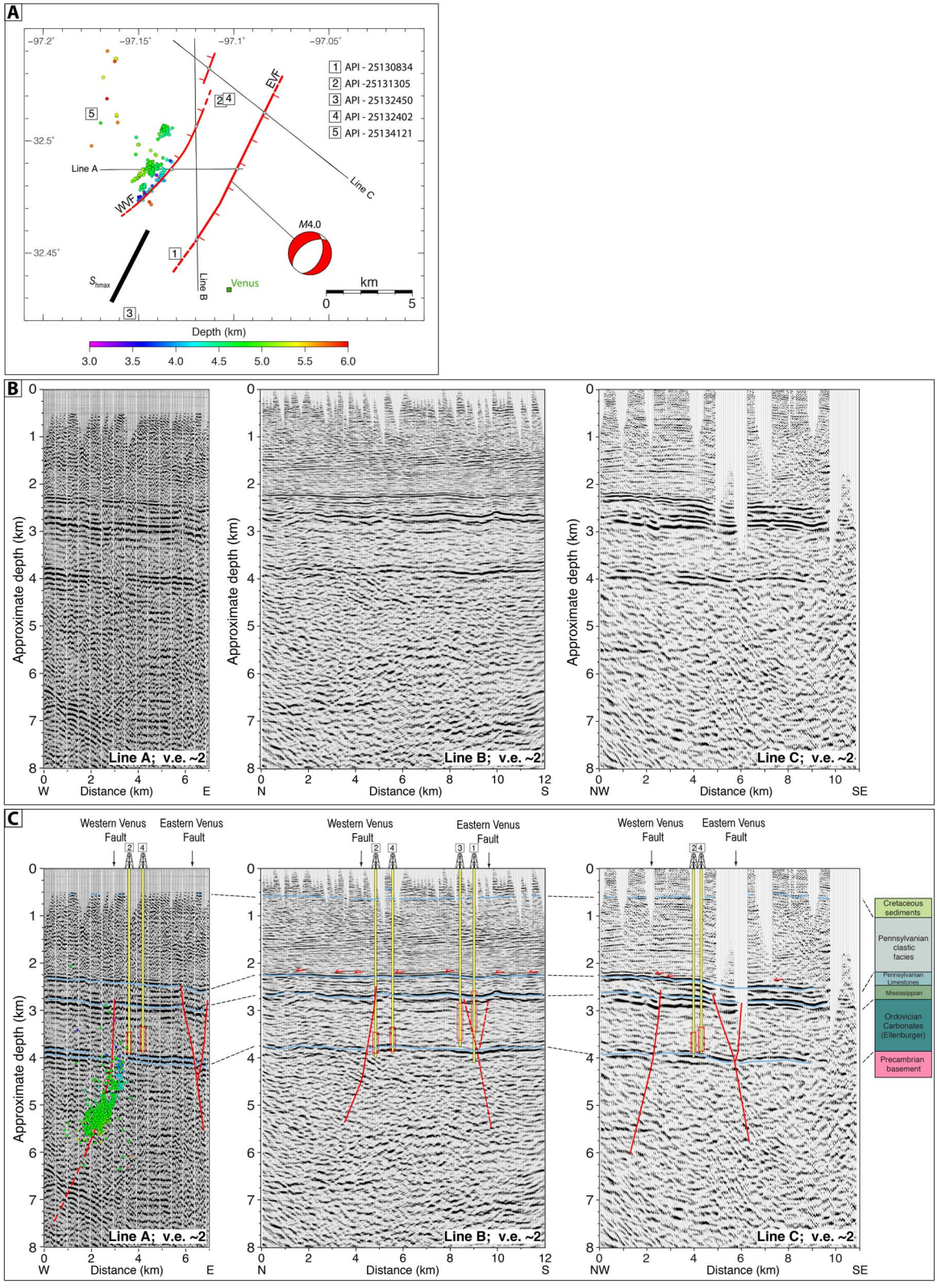

Fig. 4. Seismic reflection data in the Venus, Texas, study area. (**A**) Location map of seismic reflection profiles near Venus, Texas, Johnson County (for location, see Fig. 2), showing interpreted faults at the top of the crystalline basement, the 2008–2016 relocated seismicity (colored circles) (*32*), the ANSS moment tensor location of the 2015 M_w 4.0 event (location uncertainty ± 4.5 km). S_{Hmax} orientation from Lund Snee and Zoback (*42*). Squares are saltwater disposal wells with production well numbers [American Petroleum Institute (API)]. (**B**) Unmarked time-migrated, depth-converted seismic reflection profiles. (**C**) Interpreted seismic reflection profiles. Red rectangles on wells show saltwater disposal injection depth intervals. Hypocentral locations (green circles) were projected only along line A. See Fig. 3 for corresponding stratigraphy in the FWB.

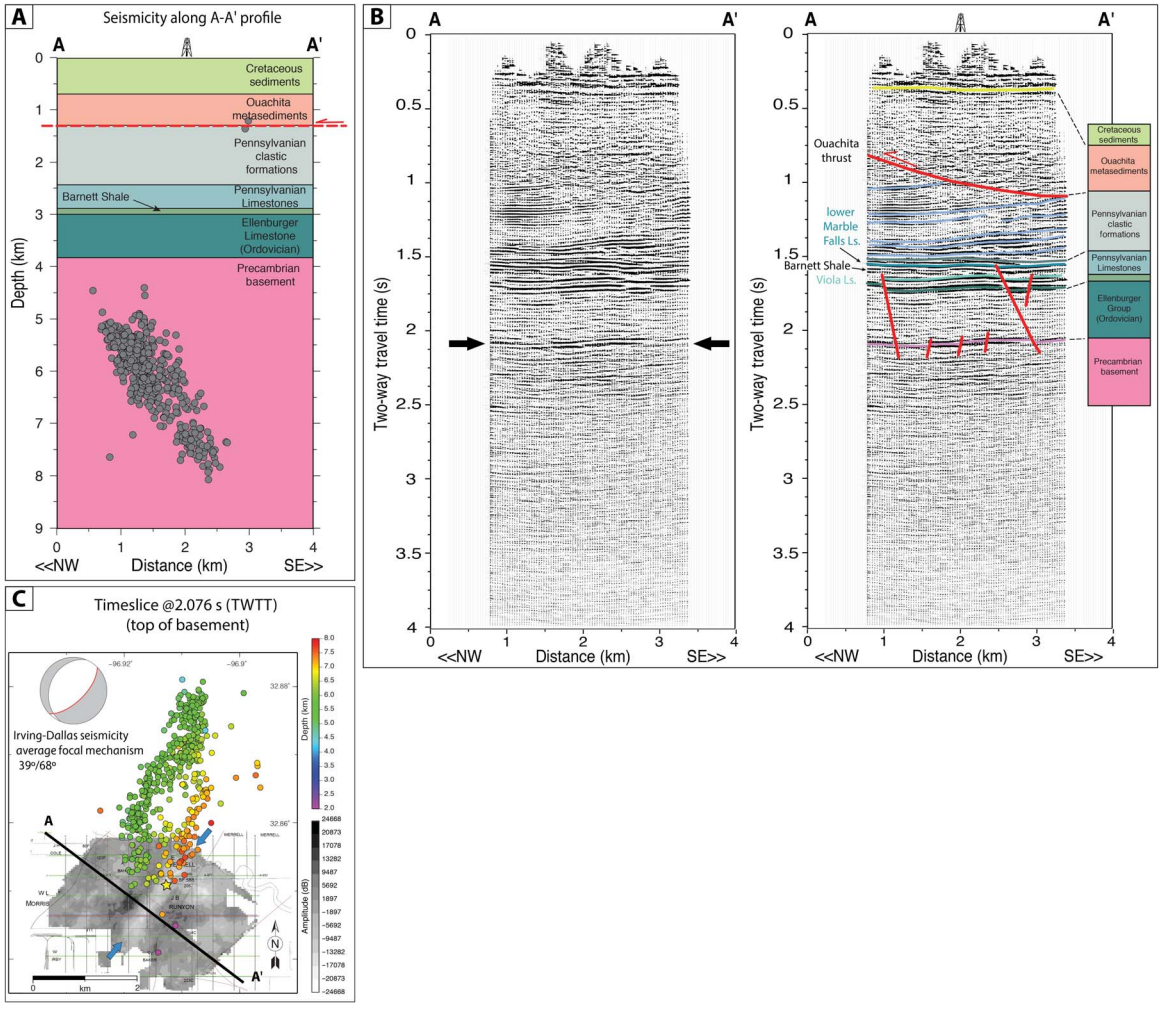

Fig. 5. Seismic reflection data in the Dallas-Irving, Texas, study area. (**A**) SMU earthquake catalog hypocentral locations projected onto the trace of the seismic profile near Irving, Texas (see map in Fig. 2). Depths of geological unit tops are based on nearby well logs. (**B**) Unmarked and interpreted time-migrated seismic reflection profile near Irving, Texas. Tops of stratigraphic units are constrained by the well ~500 m NE of the profile [star in (C)]. Black arrows show the two-way travel time (TWTT) of the horizontal time slice shown in (C). (**C**) Horizontal time slice at 2.076 s (TWTT) (normal polarity amplitude map at the top of crystalline basement) shows structures (marked by blue arrows) striking ~N40°E parallel to the general trend of the hypocenters in the basement (shown by circles, color-coded by depth) and to the average focal mechanism of the Dallas-Irving seismic sequence (N39°E). NW-SE black line shows the location of seismic profile in (B). Yellow star is the location of production well pad.

those currently active identified in the Venus area and, like in Venus, appear favorably oriented for failure in the current stress field. The continuity of post–Marble Falls reflectors above the faults, which displace the top of the Ellenburger and of the basement, indicates inactivity along these faults since the deposition of the Bend Group (circa 310 Ma) and until the recent earthquake occurrence.

The northern Mississippi embayment

Tectonic setting and seismicity

The Mississippi embayment is a southwest-dipping trough filled with Upper Cretaceous and Cenozoic clastic sediments that unconformably lie on Upper Cambrian to Ordovician sedimentary rocks and a Precambrian crystalline basement (*43*, *44*). The basin is a long-lived, fundamentally weak zone in the North American plate, and it has been the location of repeated crustal extension, compression, and continental rifting since at least the end of the Proterozoic, with several episodes of reactivation and magmatic activity (*45*). The Reelfoot rift (Fig. 6), today buried under the Mississippi valley sediments, represents the backbone of the basin (*46*) and is defined by a system of intracratonic faults that displace the top of the crystalline basement by more than 2 km along the rift margins (*47*, *48*). The rift hosts the current, historical, and prehistorical seismicity of the NMSZ, whose earthquakes are rupturing and reactivating faults of the Paleozoic aulacogen (*47*, *48*).

The NMSZ, one of the most notorious deviations from plate rigidity, was the most seismically active area in the continental United States east of the Rocky Mountains until 2008. The zone is the site of the four largest intraplate earthquakes in the United States, the 1811–1812 sequence with estimated magnitudes of 7.0 to 7.6 (*49*–*51*). Today, instrumental seismicity outlines four main arms that extend for more than 200 km from west of Memphis, Tennessee, into southern Missouri (Fig. 6). On the basis of focal mechanisms (*52*), the active faults are interpreted as a right-lateral strike-slip fault zone with a left-lateral restraining bend (*53*–*55*). According to this interpretation, the two right-lateral strike-slip faults in the NMSZ system, the 120-km-long, near-vertical Axial fault and the New Madrid North fault, are

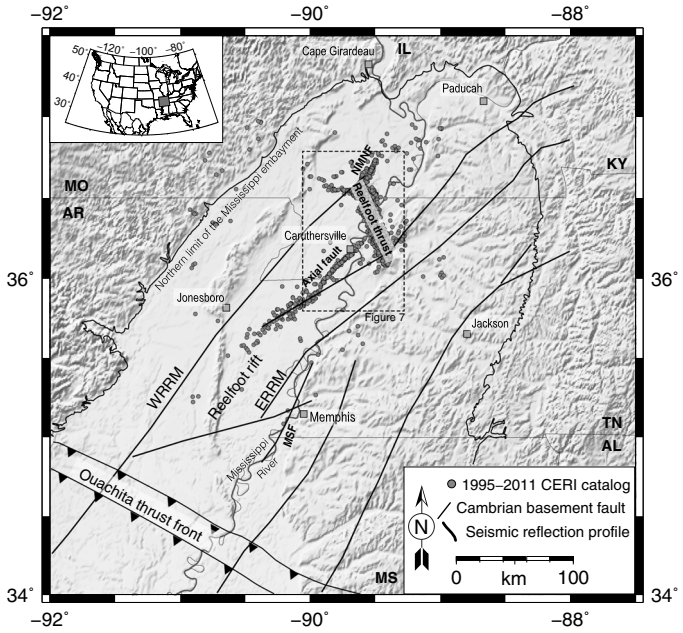

Fig. 6. The northern Mississippi embayment. The map shows the main tectonic features of the basin, the seismicity of the NMSZ [from the Center for Earthquake Research and Information (CERI) Catalog]. ERRM, eastern Reelfoot rift margin; MSF, Meeman-Shelby fault; NMNF, New Madrid North fault; WRRM, western Reelfoot rift margin. Location of Cambrian basement faults is from Thomas (*48*). Dashed rectangle shows location of Fig. 7.

connected by the southwest-dipping, 67-km-long Reelfoot thrust, which accommodates the transfer of deformation and the shortening, acting as the restraining bend (Fig. 6).

Next, we describe the deformation of two major faults in the NMSZ system (the Reelfoot thrust and the Axial fault), as imaged by seismic reflection profiles, and compare them to the example of a seismically quiescent but Holocene active fault outside the NMSZ (the Meeman-Shelby fault). These are just few of the examples emerging from three decades of high-resolution seismic exploration that reveal a pattern of long-lived Quaternary and Tertiary deformation accommodated on faults distributed across the NME (*56*–*64*).

Fault displacement history and analysis of high-resolution seismic reflection data

Reelfoot thrust

The first of these features, the Reelfoot thrust (Fig. 6), is the only seismogenic fault in the NMSZ with surface deformation, represented by a scarp and a regional uplift, a composite topographic, and structural high located on the hanging wall of the thrust. The fault crosses the meandering Mississippi River and has been mapped intermittently at the surface for ~32 km (*65*). At depth, hypocentral locations define a southwest-dipping fault that extends to 25 km with a dip varying from 30° to 45° along strike (*66*, *67*). The thrust was active in the New Madrid earthquake sequence of 1811–1812 and is interpreted to be the source of the 7 February 1812 event (M_w ~ 7.5) (*68*). The displacement history of the fault, derived from trenching and dating of the landforms over the thrust (*65*, *69*) and through the interpretation of the numerous seismic reflection surveys (*70*–*74*), reveals a long-lived history of deformation dating back to the Late Cretaceous. In particular, seismic reflection data show that geologic units in the NME, from the Paleozoic rocks through the Cenozoic sediments, are vertically offset by the thrust and displacements increase with increasing stratigraphic age. This evidence, integrated with trenching data, indicates that the Reelfoot thrust has been reactivated through time since the Cretaceous (*75*).

Axial fault

The Axial fault (*70*) is the longest fault in the seismic zone. It extends in a northeast direction for ~120 km along the axis of the Reelfoot rift. Seismicity along the Axial fault occurs between depths of 3 and 15 km on a near-vertical plane with predominant right-lateral strike-slip movement (*52*, *54*, *67*). At shallower depths, deformation is accommodated by two parallel faults, the Axial fault and the Cottonwood Grove fault, both imaged by high-resolution reflection profiles (Fig. 7) (*74*, *76*). On the basis of several lines of evidence (*50*, *77*), the Axial fault is interpreted to have ruptured during the first (16 December 1811, M_w 7.3) and possibly the second (16 December 1811, M_w 7.0) of the 1811–1812 earthquakes (*78*). Although no surface rupture has been identified for these events, they have left behind subtle vertical and large-scale horizontal deformation that resulted in sunken lands along the trace of the fault (*77*). Geomorphological evidence shows this to be the most recent deformation that began in the later part of the Pleistocene and continued through the Holocene (*77*). High-resolution marine seismic reflection data acquired along the Mississippi River image the faults as they deform the sedimentary sequences of the NME from the Quaternary alluvium to the Paleozoic rocks (Fig. 7). As with the Reelfoot thrust, the Axial fault and the Cottonwood Grove fault exhibit increasing displacement with increasing age of geologic units, indicating a prolonged history of activity during the Cenozoic (*74*).

Reelfoot rift margin

Along the eastern margin of the Reelfoot rift, ~75 km south of the NMSZ and about 10 km west of Memphis, Tennessee, high-resolution seismic reflection data image the ~45-km-long, 25°N striking Meeman-Shelby fault (*79*). The fault repeatedly crosses the meandering Mississippi River, offsets the Paleozoic rocks, and folds the overlying sediments with an up-to-the-west sense of motion. Similar to the NMSZ faults, deformation across the Meeman-Shelby fault decreases upward, suggesting repeated reactivation since the Late Cretaceous. The base of the Quaternary alluvium, marked by the upper Eocene/Quaternary contact, is folded by 28 m above the fault with a consistent sense of motion. The base of the Quaternary alluvium along the fault hanging wall was drilled, sampled, and dated at 14.3 ± 0.50 ka (thousand years ago) (*80*), confirming the recent age of fault movement. Despite its recent activity, the fault has no surface manifestation, likely due to its position within the Mississippi River meander belt that does not favor preservation of surface morphology over the long term.

DISCUSSION

The most significant result of this study is that in the FWB, a region of intense recent seismic activity and commercial wastewater injection, analysis of fault displacements expressed in seismic reflection data finds no evidence of previous active faulting for the past ~300 My (that is, after Middle Pennsylvanian deformation).

By contrast, analysis of seismic reflection data in the NME, a region where historical natural earthquakes with M_w 7+ have occurred, shows that fault displacements have been ongoing for the past ~65 My throughout the Tertiary and possibly the Cretaceous.

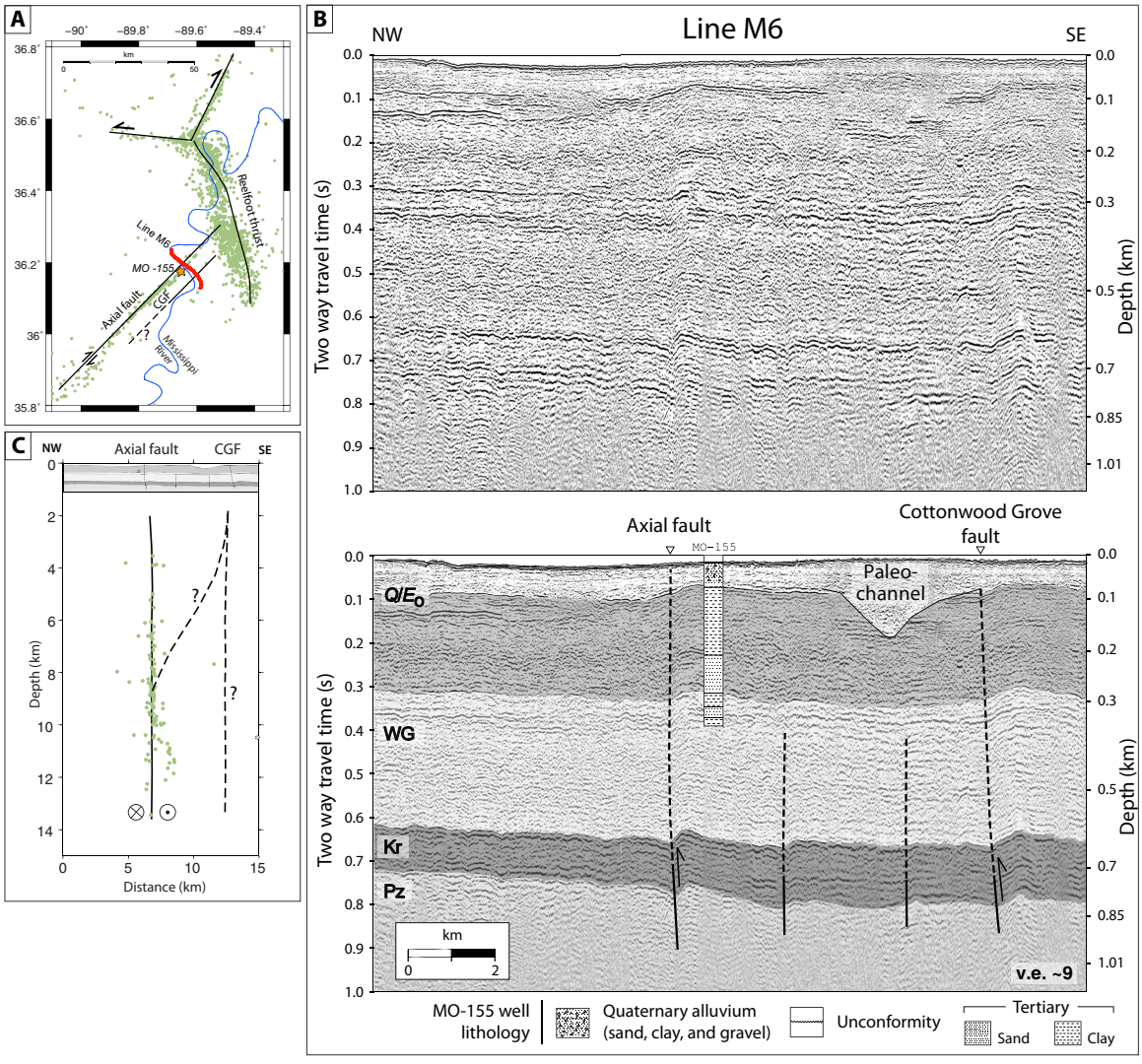

Fig. 7. Seismic reflection data across the NMSZ. (**A**) Location map of the marine seismic reflection line *M6* acquired along the Mississippi River, MO-155 well (orange star), and NMSZ seismicity (green circles). CGF, Cottonwood Grove fault. (**B**) Unmarked (top) and interpreted (bottom) seismic line *M6*. The Axial fault and the CGF deform the base of the Quaternary alluvium [marked by the Eocene/Quaternary unconformity (Q/E_o)], Cenozoic, and Mesozoic semi-consolidated sediments to the top of the Ordovician rocks. Vertical displacements increase with age of geologic unit on each fault from ~25 m at the base of the Quaternary to ~40 m at the top of the Cretaceous sediments to ~60 m at the top of the Ordovician rocks, indicating a long-lived history of deformation along both faults throughout the Cenozoic and possibly the Mesozoic (WG, Paleocene-Eocene Wilcox Group; Kr, Upper Cretaceous sediments; Pz, Ordovician sedimentary rocks). (**C**) Hypocenter locations (green circles) within 10 km of the seismic line projected onto the profile show the Axial fault as a vertical fault that extends to depths of 12 km beneath the seismic line. Focal mechanisms show predominant left-lateral strike-slip movement along the Axial fault. Whether the Axial fault and the Cottonwood Grove faults are two distinct structures at depth or part of a flower strike-slip system is still debated.

Together, these results support the assertion that recent earthquake activity in the FWB is anthropogenic. This conclusion contrasts with the interpretation by some (*81*, *82*) that recent seismicity in the FWB reflects tectonic deformation of faults that have remained active since the Paleozoic, in a fashion similar to what is observed in other intraplate regions where tectonic seismic activity appears to be episodic, migratory, and/or clustered (*9*, *11*, *12*).

The lack of displacement in units younger than the Early Pennsylvanian can be explained in either of two ways: (i) fault displacement since the Early Pennsylvanian is null or negligible, or (ii) fault displacement since the Early Pennsylvanian has occurred, but cumulative vertical slip is less than the vertical resolution of the seismic reflection data and therefore is not resolved by the data. Considerations of the seismic data sampling rate (2 ms), dominant frequency content (~60 Hz), and seismic velocity of units above the top of the Ordovician limestones with Vp (P-wave velocity) ~3.45 km/s based on the interval velocity reported by the Trigg well no. 1 (Geotechnical Corporation) (*21*, *83*) indicate a vertical resolution on the order of 15 m for the data analyzed here.

The latter option—that faults have remained active since the Pennsylvanian—can be explored by taking recent seismicity as a guide to the deformation style of the faults. Assuming that the recent seismic sequences that occurred in the FWB (that is, Azle-Reno, Venus, and Irving-Dallas) are representative of the style of recurrent deformation along the associated faults, the amount of displacement accumulated in these latest sequences can be calculated, and from that, a minimum return interval for each sequence can be derived such that the cumulative slip along each fault does not exceed an upper

bound imposed by the minimum vertical resolution of the seismic data (~15 m).

For the purposes of this calculation, two simplifying assumptions will be made: first, that faults have accumulated slip uniformly since the Pennsylvanian (that is, over the past 300 My), and second, that recent seismic sequences are representative of those that have occurred in the past along the faults. Recent seismicity is characterized by seismic swarms lasting a few months to a few years (*29*, *33*), with earthquake magnitudes not exceeding M_w 3.5 to M_w 4.0 (see table S1) and hypocenters distributed over fault areas that extend between 10 and 15 km^2, based on the SMU earthquake catalog (*19*, *29*, *32*, *33*).

We evaluated the accumulated fault displacement ΣD associated with observed earthquake activity by summing the scalar moments of earthquakes on these faults. To calculate scalar moment (M_o) for an earthquake, we assume that local magnitude (M_L) and M_w are equivalent, which is approximately true for events with M_L of 3.0 (*84*, *85*). To determine M_o, we use the equation that defines M_w in terms of M_o (*86*):

$$\log M_o = 1.5M_w + 16.0 \quad (1)$$

Then, we sum the scalar moments to determine ΣM_o, the accumulated scalar moment associated with these earthquakes. Then, from the definition of scalar moment (*87*):

$$M_o = \mu DA \quad (2)$$

we determine the accumulated fault displacement ΣD; here, μ is the rigidity of the crust (3.0×10^{11} dynes/cm^2 for relatively stiff continental crust) (*88*), D is the average slip on the fault, and A is the fault area. For the Azle-Reno, Irving-Dallas, and Venus sequences, this translates into a fault displacement of approximately 4 mm per sequence (Table 1). For repeated sequences of this type to have accumulated no more than 15 m in the past 300 My, each sequence could not have occurred more frequently than every 60,000 years on average. It is worth mentioning that fault areas as imaged by reflection data and by hypocenter distribution permit magnitudes larger than those experienced since 2008. Larger magnitudes translate to larger displacements and to longer return intervals. Therefore, we consider our estimate of return intervals using the actual magnitudes and not the maximum allowed magnitudes as a minimum value. Return intervals of ~60,000 years or more are not incompatible with strain rates in the order of 10^{-17} s^{-1} typical of intraplate regions (*10*), although they are a reminder of the rarity of each of these events. The 2D seismic data allow an unresolved component of strike-slip offset. However, any such component is likely minor, given that recent FWB seismicity is almost purely dip-slip and—as we argue below—faulting has occurred within a stress field that is likely unchanged over the past 200 My or more.

It is reasonable to assume that these three seismic sequences are occurring independently, and that earthquakes in one sequence are not triggering those in a different sequence through static stress changes, considering that the average fault rupture length (~6 km) is one order of magnitude shorter than the distance between the sequences (~50 to 60 km). If each independent sequence recurs every 60,000 years, then the probability of any one of these sequences to develop in the past 10 years (or since 2008) is ~0.017% (that is, 1 in 6000). The probability drops to 1 in 6×10^7 for two sequences to occur independently and concurrently within 10 years, and the occurrence of three sequences during the same time period is even less likely. Since 2008, the FWB has witnessed the occurrence of, at minimum, five well-documented sequences producing M_w 3+ earthquakes on different faults (*19*, *21*, *27*, *28*, *32*), which represent an exceedingly unlikely occurrence even for intraplate regions. These probabilities would be even lower if recurrence intervals are longer than our calculated maximum of ~60,000 years.

On the basis of these observations, we must reject the hypothesis that these earthquake swarms are being triggered by tectonic forces. Rather, the data indicate that the FWB faults have experienced a remarkable lack of deformation in the past ~300 My, until the recent 2008 surge in seismicity, and independently confirm the interpretation by other authors of the recent seismic sequences in the FWB as induced rather than natural.

Zoback (*89*) has suggested that recent industry operations are simply accelerating the occurrence of earthquakes that would have naturally occurred over hundreds or thousands of years. This hypothesis stems from the work of Zoback and Townend (*5*), who argued that some amount of continual faulting is necessary to maintain sufficient permeability to equilibrate crustal fluid pressures at the observed hydrostatic levels. Zoback's hypothesis is compatible with our observations in the NME, where faults are seen to have been active over millions of years. However, it is incompatible with our observations for the FWB, where the faults responsible for recent seismicity appear to have been mostly to entirely inactive since the Pennsylvanian. The seismic data do not reveal how far these faults lie from failure: Our only insight comes from the fact that they failed recently, and therefore, they must have been close to failure, a conclusion that aligns with

Table 1. Recurrence interval calculation for currently active FWB seismic sources. Fault dimensions were derived from the SMU earthquake catalog and detailed studies (*19*, *32*). Seismic moment for each sequence was calculated using NEIC catalog local magnitudes (M_{b_lg}) (see table S1). Note that fault areas allow for larger maximum magnitudes than those recorded by the current seismic sequences (*98*). Larger magnitudes would translate into larger slip/sequence and therefore into longer return intervals for each seismic sequence. Therefore, by assuming that current seismic sequences are representative of past slip occurrences, our estimates for return times can be considered minimum values.

Sequence	Strike of fault	Dip of fault	Along-strike extent (km)	Down-dip extent (km)	Faulted area (km^2)	Moment of sequence (dynes × cm)	Fault displacement in sequence (cm)	Maximum number of sequences	Minimum recurrence interval (years)
Azle	225	70	3.5	4.3	14.9	2.11×10^{22}	0.39	3804	78,866
Irving	39	68	3.5	4.3	15.1	1.49×10^{22}	0.28	5454	55,003
Venus	220	56	5.5	2.4	13.3	1.18×10^{22}	0.25	6068	49,440

evidence showing that many intraplate faults are stressed close to criticality (*5*).

Last, a note should be added regarding the time scale of changes of the regional stress field responsible for fault offsets. Although the faults analyzed in this study are favorably oriented for failure in the modern stress field, it is likely that this stress field did not persist unchanged for the past 300 My. The state of stress in the earth's lithosphere is the result of the superposition of forces deriving from many different processes. In general, however, the dominant forces responsible for broad stress patterns are best explained by plate tectonic forces (*90*), and the stress fields derived from these forces change over time periods comparable to those between major plate reorganizations. For example, along the Atlantic Coastal Plain, the consistent style of observed fault offsets along this passive margin suggests a similar stress field for the past ~110 My (*91*, *92*), whereas in areas near plate boundaries, such as the western United States, the stress field may change as often as the relative plate motion or plate boundary configuration. For north Texas and the FWB, as well as for the northern Gulf of Mexico continental margin and Coastal Plains, the main post-orogenic (Ouachita) stress field change is associated with the breakup of Pangea (*48*, *93*), which led to the rifting of the Gulf of Mexico starting in the Late Triassic (~228 to 210 Ma) (*94*, *95*) and ending in the Late Jurassic–Early Cretaceous (~154 to 149 Ma) (*94*, *95*). Today, S_{Hmax} along the Gulf coast of southern Texas, Louisiana, and eastern Mexico is subparallel to the coastline, where growth faulting accommodates extension of the post-Jurassic sedimentary sequences into the Gulf of Mexico (*42*, *96*). From this, we conclude that the state of stress acting on the faults of the FWB has persisted for at least the last 200 My.

In summary, a comparison between seismic reflection data across active faults in the CUS intraplate region shows that faults in areas where deformation is unequivocally caused by tectonic processes (for example, the NMSZ in the NME and surrounding region) display resolvable deformation of Cenozoic and Quaternary units. In some cases, fault offsets increase with stratigraphic age, documenting a long-lived tectonic activity of the fault. In contrast, seismic reflection images across seismically active faults in the FWB, north Texas, analyzed in this study show that faults displace the top of the Precambrian crystalline basement and the overlying Early Ordovician Ellenburger Group through the Lower Pennsylvanian Marble Falls Limestone, including the Mississippian Barnett Shale, but extend no higher in the section. No post–Early Pennsylvanian deformation is resolved by the seismic reflection data on currently active faults. Specifically, any vertical displacements in the post–Early Pennsylvanian units are below the vertical resolution of the seismic data at these depths (~15 m), far less than expected had these faults accumulated deformation over the long term. Assuming that current seismicity recorded in the FWB is representative of past seismic sequences, a cumulative vertical displacement equal to or less than 15 m along the currently active faults implies an average recurrence interval of 60,000 years or longer, based on the average displacement/sequence derived from cumulative seismic moment calculations of current seismicity. These exceptionally long time intervals are at odds with the increasing number of faults reactivated in the basin (five identified and seismically monitored seismic sequences since 2008).

Our analysis indicates that faults in the FWB have been inactive for the past ~300 My, until the recent 2008 surge in seismicity. The results are consistent with previous studies and inconsistent with a suggested sustained, significant Mesozoic and Cenozoic activity in the basin along these faults. Rather, the results, solely based on structural analysis of seismic reflection data and largely independent of recent seismicity and correlation with wastewater injection, strongly suggest that the recent seismicity in the FWB is highly anomalous and therefore more likely induced than natural. The alternative, unlikely case that the modern seismicity observed in the FWB is the effect of the exceptionally long rupture cycle of naturally active intraplate faults calls into question industry strategies that involve injections of large volumes of fluid at high rates near favorably oriented, critically stressed, active faults.

MATERIALS AND METHODS

Seismic reflection profiles in the Venus, Texas, region were provided by the USGS Earthquake Hazards Program. Seismic reflection data in the Irving, Texas, region are proprietary. Seismic reflection data in the NME were downloaded from the University of Texas Institute for Geophysics seismic data portal. Class II underground injection control (UIC) saltwater disposal API well identification number, location, and injection depth interval data were provided by the Texas Railroad Commission. The USGS NEIC earthquake database provided the earthquake locations and magnitudes used in this study for the recurrence calculations.

SUPPLEMENTARY MATERIALS

Supplementary material for this article is available at http://advances.sciencemag.org/cgi/content/full/3/11/e1701593/DC1

table S1. USGS NEIC earthquake catalog.

table S2. Seismic reflection data parameters for lines A, B, and C in Johnson County, Texas, and Irving, Texas.

REFERENCES AND NOTES

1. W. L. Ellsworth, Injection-induced earthquakes. *Science* **341**, 1225942 (2013).
2. K. M. Keranen, H. M. Savage, G. A. Abers, E. S. Cochran, Potentially induced earthquakes in Oklahoma, USA: Links between wastewater injection and the 2011 M_w 5.7 earthquake sequence. *Geology* **41**, 699–702 (2013).
3. W.-Y. Kim, Induced seismicity associated with fluid injection into a deep well in Youngstown, Ohio. *J. Geophys. Res. Solid Earth* **118**, 3506–3518 (2013).
4. J. Townend, M. D. Zoback, How faulting keeps the crust strong. *Geology* **28**, 399–402 (2008).
5. M. D. Zoback, J. Townend, Implications of hydrostatic pore pressures and high crustal strength for the deformation of intraplate lithosphere. *Tectonophysics* **336**, 19–30 (2001).
6. T. H. Dixon, A. Mao, S. Stein, How rigid is the stable interior of the North American plate? *Geophys. Res. Lett.* **23**, 3035–3038 (1996).
7. E. Calais, J. Y. Han, C. DeMets, J. M. Nocquet, Deformation of the North American plate interior from a decade of continuous GPS measurements. *J. Geophys. Res.* **111**, B06402 (2006).
8. H. Wang, M. Liu, J. Cao, X. Shen, G. Zhang, Slip rates and seismic moment deficits on major active faults in mainland China. *J. Geophys. Res.* **116**, B02405 (2011).
9. A. J. Crone, P. M. De Martini, M. N. Machette, K. Okumura, J. R. Prescott, Paleoseismicity of two historically quiescent faults in Australia: Implications for fault behavior in stable continental regions. *Bull. Seismol. Soc. Am.* **93**, 1913–1934 (2003).
10. R. T. Williams, L. B. Goodwin, W. D. Sharp, P. S. Mozley, Reading a 400,000-year record of earthquake frequency for an intraplate fault. *Proc. Natl. Acad. Sci. U.S.A.* **114**, 4893–4898 (2017).
11. A. J. Crone, M. N. Machette, J. R. Bowman, Episodic nature of earthquake activity in stable continental regions revealed by paleoseismicity studies of Australian and North American Quaternary faults. *Aust. J. Earth Sci.* **44**, 203–214 (1997).
12. M. Liu, S. Stein, H. Wang, 2000 years of migrating earthquakes in North China: How earthquakes in midcontinents differ from those at plate boundaries. *Lithosphere* **3**, 128–132 (2011).
13. J. L. Rubinstein, A. B. Mahani, Myths and facts on wastewater injection, hydraulic fracturing, enhanced oil recovery, and induced seismicity. *Seismol. Res. Lett.* **86**, 1060–1067 (2015).
14. M. D. Petersen, C. S. Mueller, M. P. Moschetti, S. M. Hoover, A. L. Llenos, W. L. Ellsworth, A. J. Michael, J. L. Rubinstein, A. F. McGarr, K. S. Rukstales, Seismic-hazard forecast for

2016 including induced and natural earthquakes in the central and eastern United States. *Seismol. Res. Lett.* **87**, 1327–1341 (2016).
15. M. Weingarten, S. Ge, J. W. Godt, B. A. Bekins, J. L. Rubinstein, High-rate injection is associated with the increase in U.S. mid-continent seismicity. *Science* **248**, 1336–1340 (2015).
16. S. Horton, Disposal of hydrofracking waste fluid by injection into subsurface aquifers triggers earthquake swarm in central Arkansas with potential for damaging earthquake. *Seismol. Res. Lett.* **83**, 250–260 (2012).
17. L. V. Block, C. K. Wood, W. L. Yeck, V. M. King, The 24 January 2013 M_L 4.4 earthquake near Paradox, Colorado, and its relation to deep well injection. *Seismol. Res. Lett.* **85**, 609–624 (2014).
18. K. M. Keranen, M. Weingarten, G. A. Abers, B. A. Bekins, S. Ge, Sharp increase in central Oklahoma seismicity since 2008 induced by massive wastewater injection. *Science* **345**, 448–451 (2014).
19. M. J. Hornbach, H. R. DeShon, W. L. Ellsworth, B. W. Stump, C. Hayward, C. Frohlich, H. R. Oldham, J. E. Olson, M. B. Magnani, C. Brokaw, J. H. Luetgert, Causal factors for seismicity near Azle, Texas. *Nat. Commun.* **6**, 6728 (2015).
20. S. M. Mousavi, P. O. Ogwari, S. P. Horton, C. A. Langston, Spatio-temporal evolution of frequency-magnitude distribution and seismogenic index during initiation of induced seismicity at Guy-Greenbrier, Arkansas. *Phys. Earth Planet. Inter.* **267**, 53–66 (2017).
21. C. Frohlich, C. Hayward, B. Stump, E. Potter, The Dallas–Fort Worth earthquake sequence: October 2008 through May 2009. *Bull. Seismol. Soc. Am.* **101**, 327–340 (2011).
22. C. Frohlich, Two-year survey comparing earthquake activity and injection-well locations in the Barnett Shale, Texas. *Proc. Natl. Acad. Sci. U.S.A.* **109**, 13934–13938 (2012).
23. C. Frohlich, H. DeShon, B. Stump, C. Hayward, M. Hornbach, J. L. Walter, A historical review of induced earthquakes in Texas. *Seismol. Res. Lett.* **87**, 1022–1038 (2016).
24. R. M. Pollastro, D. M. Jarvie, R. J. Hill, C. W. Adams, Geologic framework of the Mississippian Barnett Shale, Barnett-Paleozoic total petroleum system, Bend arch Fort Worth Basin, Texas. *Am. Assoc. Petrol. Geol. Bull.* **91**, 405–436 (2007).
25. M. J. Guccione, Late Pleistocene and Holocene paleoseismology of an intraplate seismic zone in a large alluvial valley, the New Madrid seismic zone, Central USA. *Tectonophysics* **408**, 237–264 (2005).
26. M. P. Tuttle, E. S. Schweig, J. D. Sims, R. H. Lafferty, L. W. Wolf, M. L. Haynes, The earthquake potential of the New Madrid seismic zone. *Bull. Seismol. Soc. Am.* **92**, 2080–2089 (2002).
27. A. H. Justinic, B. H. Stump, C. Hayward, C. Frohlich, Analysis of the Cleburne, Texas earthquake sequence from June 2009 to June 2010. *Bull. Seismol. Soc. Am.* **103**, 3083–3093 (2013).
28. M. J. Hornbach, M. Jones, M. Scales, H. R. DeShon, M. B. Magnani, C. Frohlich, B. Stump, C. Hayward, M. Layton, Ellenburger wastewater injection and seismicity in North Texas. *Phys. Earth Planet. Inter.* **261**, 54–68 (2016).
29. H. R. DeShon, M. B. Magnani, *North Texas Earthquake Studies and Network Operations* (Open File Report #G15AC00141, U.S. Geological Survey, 2016).
30. H. R. DeShon, M. Scales, C. Hayward, M. J. Hornbach, M. B. Magnani, B. Stump, C. Frohlich, J. Walter, Comparison study between North Texas Earthquake sequences from 2008–2015, paper presented at the 2015 Fall Meeting, American Geophysical Union, San Francisco, CA, 14 to 18 December 2015.
31. L. Quinones, H. R. DeShon, C. Hayward, M. Scales, Characterization of the 2015 Dallas-Irving Earthquake Sequence, paper presented at the 2015 Fall Meeting, American Geophysical Union, San Francisco, CA, 14 to 18 December 2015.
32. M. Scales, "A decade of induced slip on the causative fault of the 2015 M_w 4.0 Venus earthquake, northeast Johnson County Texas," thesis, Southern Methodist University (2017).
33. R. H. DeShon, M. B. Magnani, *Imaging Faults in Induced Earthquake Zones Using Earthquake and Controlled Source Data—North Texas and Northern Oklahoma* (Open File Report #G16AC00247, U.S. Geological Survey, 2017).
34. W. A. Thomas, G. W. Viele, J. K. Arbenz, R. L. Nicholas, R. E. Denison, W. R. Muehlberger, P. R. Tauvers, Tectonic map of the Ouachita orogen, and cross sections of the Appalachian-Ouachita orogen beneath the Gulf Coastal Plain, in *The Appalachian-Ouachita Orogen in the United States*, R.D. Hatcher Jr., W.A. Thomas, G.W. Viele, Eds. (Geological Society of America, 1989).
35. J. L. Walper, Plate tectonic evolution of the Fort Worth Basin, in *Petroleum Geology of the Fort Worth Basin and Bend Arch Area*, C. A. Martin, Ed. (Dallas Geological Society, 1982), pp. 237–251.
36. T. E. Ewing, R. T. Budnik, J. T. Ames, D. M. Ridner, R. Dillon, *Tectonic Map of Texas* (Bureau of Economic Geology, University of Texas at Austin, 1990).
37. N. M. Rach, Drilling expands in Texas' largest gas field. *Oil Gas J.* **102**, 45–50 (2004).
38. M. Kathiwada, G. R. Keller, K. J. Marfurt, A window into the Proterozoic: Integrating 3D seismic, gravity, and magnetic data to image subbasement structures in the southeast Fort Worth basin. *Interpretation* **1**, T125–T141 (2013).
39. E. C. Sullivan, K. J. Marfurt, A. Lacazette, M. Ammerman, Application of new seismic attributes to collapse chimneys in the Fort Worth basin. *Geophysics* **71**, B111–B119 (2006).
40. D. W. Browning, Geology of the North Caddo area, Stephens County, Texas, in *Petroleum Geology of the Fort Worth Basin and Bend Arch Area*, C. A. Martin, Ed. (Dallas Geological Society, 1982), pp. 315–330.
41. J. W. Flippin, The stratigraphy, structure, and economic aspects of the Paleozoic strata in Erath County, north central Texas, in *Petroleum Geology of the Fort Worth Basin and Bend Arch Area*, C. A. Martin, Ed. (Dallas Geological Society, 1982), pp.129–155.
42. J.-E. Lund Snee, M. D. Zoback, State of stress in Texas: Implications for induced seismicity. *Geophys. Res. Lett.* **43,** 10208–10214 (2016).
43. R. G. Stearns, Cretaceous, Paleocene, and Lower Eocene: Geologic history of the Northern Mississippi Embayment. *Geol. Soc. Am. Bull.* **68**, 1077–1100 (1957).
44. W. J. Autin, S. F. Burns, B. J. Miller, R. T. Saucier, J. I. Snead, Quaternary geology of the Lower Mississippi Valley, in *Quaternary Nonglacial Geology: Conterminous United States*, R. B. Morrison, Ed. (Geological Society of America, 1991), pp. 547–582.
45. C. P. Ervin, L. D. McGinnis, Reelfoot rift: Reactivated precursor to the Mississippi embayment. *Geol. Soc. Am. Bull.* **86**, 1287–1295 (1975).
46. T. G. Hildenbrand, J. D. Hendricks, *Geophysical Setting of the Reelfoot Rift and Relations Between Rift Structures and the New Madrid Seismic Zone* (Professional Paper 1538-E, U.S. Geological Survey, 1995), pp. 1–30.
47. M. F. Kane, T. G. Hildenbrand, J. D. Hendricks, Model for the tectonic evolution of the Mississippi embayment and its contemporary seismicity. *Geology* **9**, 563–568 (1981).
48. W. A. Thomas, The lapetan rifted margin of southern Laurentia. *Geosphere* **7**, 97–120 (2011).
49. O. W. Nuttli, The Mississippi Valley earthquakes of 1811 and 1812: Intensities, ground motion, and magnitudes. *Bull. Seismol. Soc. Am.* **63**, 227–248 (1973).
50. A. C. Johnston, E. S. Schweig, The enigma of the New Madrid earthquakes of 1811–1812. *Annu. Rev. Earth Planet. Sci.* **24**, 339–384 (1996).
51. S. E. Hough, J. G. Armbruster, L. Seeber, J. F. Hough, On the modified Mercalli intensities and magnitudes of the 1811–1812 New Madrid, central U.S. earthquakes. *J. Geophys. Res.* **105**, 23839–23864 (2000).
52. G. A. Johnson, S. P. Horton, M. Withers, R. T. Cox, Earthquake focal mechanisms in the New Madrid seismic zone. *Seismol. Res. Lett.* **85**, 257–267 (2014).
53. D. P. Russ, Style and significance of surface deformation in the vicinity of New Madrid, Missouri, in *Investigations of the New Madrid, Missouri, Earthquake Region*, F. A. McKeown, L. C. Pakiser, Eds. (Professional Paper 1236, U.S. Geological Survey, 1982), pp. 95–114.
54. J. M. Chiu, A. C. Johnston, Y. T. Yang, Imaging of the active faults of the central New Madrid seismic zone using PANDA array data. *Seismol. Res. Lett.* **63**, 375–393 (1992).
55. T. L. Pratt, Kinematics of the New Madrid seismic zone, central United States, based on stepover models. *Geology* **40**, 371–374 (2012).
56. E. S. Schweig III, R. T. Marple, The Bootheel lineament: A possible coseismic fault of the great New Madrid earthquakes. *Geology* **19**, 1025–1028 (1991).
57. E. A. Luzietti, L. R. Kanter, E. S. Schweig III, K. M. Shedlock, R. B. Van Arsdale, *Shallow Deformation Along the Crittenden Country Fault Zone Near the Southeastern Margin of the Reelfoot Rift, Northeastern Arkansas* (Professional Paper 1538-J, U.S. Geological Survey, 1995).
58. R. A. Williams, E. A. Luzietti, D. L. Carver, High-resolution seismic imaging of Quaternary faulting on the Crittenden County fault zone, New Madrid seismic zone, northeastern Arkansas. *Seismol. Res. Lett.* **66**, 42–57 (1995).
59. R. W. Harrison, D. Hoffman, J. D. Vaughn, J. R. Palmer, C. L. Wiscombe, J. P. McGeehin, W. J. Stephenson, J. K. Odum, R. A. Williams, S. L. Forman, An example of neotectonism in a continental interior-Thebes Gap, Midcontinent, United States. *Tectonophysics* **305**, 399–417 (1999).
60. R. A. Williams, W. J. Stephenson, J. K. Odum, D. M. Worley, Seismic-reflection imaging of Tertiary faulting and related post-Eocene deformation 20 km north of Memphis, Tennessee. *Eng. Geol.* **62**, 79–90 (2001).
61. J. K. Odum, W. J. Stephenson, R. A. Williams, J. A. Devera, J. R. Staub, Near-surface faulting and deformation overlying the commerce geophysical lineament in Southern Illinois. *Seismol. Res. Lett.* **73**, 687–697 (2002).
62. J. N. Baldwin, J. B. Harris, R. B. Van Arsdale, R. Givle, K. I. Kelson, J. L. Sexton, M. Lake, Constraints on the location of the Late Quaternary Reelfoot and New Madrid North faults in the northern New Madrid seismic zone, central United States. *Seismol. Res. Lett.* **76**, 772–789 (2005).
63. R. T. Cox, J. Cherryhomes, J. B. Harris, D. Larsen, R. B. Van Arsdale, S. L. Forman, Paleoseismology of the southeastern Reelfoot Rift in western Tennessee and implications for intraplate fault zone evolution. *Tectonics* **25**, TC3019 (2006).
64. J. B. Harris, J. L. Sorrells, Shear-wave seismic reflection images of the Big Creek fault zone near Helena, Arkansas, *SEG Tech. Program Expanded Abstr.*, 1500–1503 (2006).
65. R. B. Van Arsdale, K. I. Kelson, C. H. Lumsden, Northern extension of the Tennessee Reelfoot scarp into Kentucky and Missouri. *Seismol. Res. Lett.* **65**, 57–62 (1995).
66. K. Mueller, J. Pujol, Three-dimensional geometry of the Reelfoot blind thrust: Implications for moment release and earthquake magnitude in the New Madrid seismic zone. *Bull. Seismol. Soc. Am.* **91**, 1563–1573 (2001).
67. M. Dunn, S. Horton, H. R. DeShon, C. Powell, High-resolution earthquake relocation in the New Madrid seismic zone. *Seismol. Res. Lett.* **81**, 406–413 (2010).

68. J. K. Odum, W. J. Stephenson, K. M. Shedlock, T. L. Pratt, Near-surface structural model for deformation associated with the February 7, 1812, New Madrid, Missouri, earthquake. *Geol. Soc. Am. Bull.* **110**, 149–162 (1998).
69. K. I. Kelson, R. B. Van Arsdale, G. D. Simpson, W. R. Lettis, Assessment of the style and timing of surficial deformation along the central Reelfoot scarp. Lake County, Tennessee. *Seismol. Res. Lett.* **63**, 349–356 (1992).
70. R. M. Hamilton, M. D. Zoback, Tectonic features of the New Madrid seismic zone from seismic-reflection profiles, in *Investigations of the New Madrid, Missouri Earthquake Region*, F. A. McKeown, L. C. Pakiser, Eds. (Professional Paper 1236, U.S. Geological Survey, 1982).
71. K. M. Shedlock, S. T. Harding, Mississippi River seismic survey. *Geophys. Res. Lett.* **9**, 1275–1278 (1982).
72. J. L. Sexton, P. B. Jones, Evidence for recurrent faulting in the New Madrid seismic zone from Mini-Sosie high-resolution reflection data. *Geophysics* **51**, 1760–1788 (1986).
73. R. B. Van Arsdale, J. Purser, W. Stephenson, J. K. Odum, Faulting along the Southern Margin of Reelfoot Lake, Tennessee. *Bull. Seismol. Soc. Am.* **88**, 131–139 (1998).
74. L. Guo, M. B. Magnani, K. McIntosh, B. Waldron, Quaternary deformation and fault structure in the Northern Mississippi Embayment as imaged by near-surface seismic reflection data. *Tectonics* **33**, 807–823 (2014).
75. R. B. Van Arsdale, Displacement history and slip rate on the Reelfoot fault of the New Madrid seismic zone. *Eng. Geol.* **55**, 219–226 (2000).
76. W. J. Stephenson, K. M. Shedlock, J. K. Odum, *Characterization of the Cottonwood Grove and Ridgely Faults Near Reelfoot Lake, Tennessee, from High-Resolution Seismic Reflection Data* (Professional Paper 1538-1, U.S. Geological Survey, 1995).
77. M. J. Guccione, R. B. Van Arsdale, L. H. Hehr, Origin and age of the Manila high and associated Big Lake "sunklands" in the New Madrid seismic zone, northeastern Arkansas. *Geol. Soc. Am. Bull.* **112**, 579–590 (2000).
78. K. Mueller, S. E. Hough, R. Bilham, Analysing the 1811–1812 New Madrid earthquakes with recent instrumentally recorded aftershocks. *Nature* **429**, 284–288 (2004).
79. Y. Hao, M. B. Magnani, K. McIntosh, B. Waldron, L. Guo, Quaternary deformation along the Meeman-Shelby Fault near Memphis, Tennessee, imaged by high-resolution marine and land seismic reflection profiles. *Tectonics* **32**, 501–515 (2013).
80. A. Ward, R. C. Counts, R. Van Arsdale, D. Larsen, S. A. Mahan, Quaternary displacement rates on the Meeman-Shelby fault and Joiner ridge horst, Eastern Arkansas: Results from coring Mississippi River alluvium. *Seismol. Res. Lett.* **88** (2017).
81. E. Janska, L. Eisner, Ongoing seismicity in the Dallas-Fort Worth area, Abstract 0995-1, Society of Exploration Geophysicists 2012 Annual Meeting, Las Vegas, Nevada, 2012.
82. E. Janská, L. Eisner, Ongoing seismicity in the Dallas-Fort Worth area. *Leading Edge* **31**, 1462–1468 (2012).
83. Geotechnical Corporation, *Deep-Hole Site Report, Trigg No. 1, Dallas County, Texas* (Technical Report 64-100, Geotechnical Corporation, 1964).
84. P. Gasperini, B. Lolli, G. Vannucci, Empirical calibration of local magnitude data sets versus moment magnitude in Italy. *Bull. Seismol. Soc. Am.* **103**, 2227–2246 (2013).
85. M. Di Bona, A local magnitude scale for crustal earthquakes in Italy. *Bull. Seismol. Soc. Am.* **106**, 242–258 (2016).
86. T. C. Hanks, H. Kanamori, A moment magnitude scale. *J. Geophys. Res.* **84,** 2348–2350 (1979).
87. K. Aki, Generation and propagation of G waves from the Niigata earthquake of June 16, 1964. Part 2. Estimation of earthquake moment, released energy and stress–strain drop for the G wave spectrum. *Bull. Earthquake Res. Inst. Tokyo Univ.* **43**, 73–88 (1966).
88. D. L. Turcotte, G. Schubert, *Geodynamics: Applications of Continuum Physics to Geophysical Problems* (Wiley, 1982).
89. M. D. Zoback, Managing the seismic risk posed by wastewater disposal. *Earth*, 38–43 (2012).
90. R. M. Richardson, S. C. Solomon, N. H. Sleep, Tectonic stress in the plates. *Rev. Geophys. Space Phys.* **17** 981–1019 (1979).
91. M. L. Zoback, M. Zoback, State of stress in the conterminous United States. *J. Geophys. Res.* **85**, 6113–6156 (1980).
92. C. M. Wentworth, M. Mergner-Keefer, *Regenerate Faults of Small Cenozoic Offset; Probable Earthquake Sources in the Southeastern U.S.* (Open File Report 81-356, U.S. Geological Survey, 1981).
93. J. L. Pindell, J. F. Dewey, Permo-Triassic reconstruction of western Pangea and the evolution of the Gulf of Mexico/Caribbean region. *Tectonics* **1**, 179–211 (1982).
94. G. Marton, R. T. Buffler, Jurassic reconstruction of the Gulf of Mexico Basin. *Int. Geol. Rev.* **36** 545–586 (1994).
95. M. R. Hudec, I. O. Norton, M. P. A. Jackson, F. J. Peel, Jurassic evolution of the Gulf of Mexico salt basin. *Am. Assoc. Petrol. Geol. Bull.* **97**, 1683–1710 (2013).
96. O. Heidbach, M. Rajabi, K. Reiter, M. Ziegler, *World Stress Map 2016* (GFZ Data Services, 2016).
97. T. E. Ewing, Mississippian Barnett Shale, Fort Worth basin, north-central Texas: Gas-shale play with multi-trillion cubic foot potential: Discussion. *Am. Assoc. Petrol. Geol. Bull.* **90**, 963–966 (2006).
98. D. L. Wells, K. J. Coppersmith, New empirical relationships among magnitude, rupture length, rupture width, rupture area, and surface displacement. *Bull. Seismol. Soc. Am.* **84**, 974–1002 (1994).

Acknowledgments: We thank C. Frohlich, P. Hennings, W. Mooney, R. Williams, and two anonymous reviewers for the insightful comments that greatly improved the paper. **Funding:** This research was supported by USGS Earthquake Hazards Program Cooperative Agreement G15C00141 and G16AC00247 to M.B.M. and H.R.D. **Author contributions:** M.B.M. interpreted the seismic reflection data in this study. M.L.B. developed the fault recurrence interval calculations using the ANSS earthquake catalog. H.R.D. produced the SMU earthquake catalog. M.B.M., H.R.D., M.L.B., and M.J.H. analyzed and interpreted the seismicity data. M.B.M. wrote the manuscript with comments from all other authors. **Competing interests:** The authors declare that they have no competing interests. **Data and materials availability:** All data needed to evaluate the conclusions in the paper are present in the paper and/or the Supplementary Materials. Additional data related to this paper may be requested from the authors.

Submitted 13 May 2017
Accepted 27 October 2017
Published 24 November 2017
10.1126/sciadv.1701593

Citation: M. B. Magnani, M. L. Blanpied, H. R. DeShon, M. J. Hornbach, Discriminating between natural versus induced seismicity from long-term deformation history of intraplate faults. *Sci. Adv.* **3**, e1701593 (2017).

Science Advances

Discriminating between natural versus induced seismicity from long-term deformation history of intraplate faults

Maria Beatrice Magnani, Michael L. Blanpied, Heather R. DeShon and Matthew J. Hornbach

Sci Adv **3** (11), e1701593.
DOI: 10.1126/sciadv.1701593